Published OnlineFirst June 24, 2013; DOI: 10.1158/0008-5472.CAN-13-1429

Cancer Research

Inhibition of AMPK and Krebs Cycle Gene Expression Drives Metabolic Remodeling of *Pten*-Deficient Preneoplastic Thyroid Cells

Valeria G. Antico Arciuch, Marika A. Russo, Kristy S. Kang, et al.

Cancer Res 2013;73:5459-5472. Published OnlineFirst June 24, 2013.

Published OnlineFirst June 24, 2013; DOI: 10.1158/0008-5472.CAN-13-1429

Inhibition of AMPK and Krebs Cycle Gene Expression Drives Metabolic Remodeling of *Pten*-Deficient Preneoplastic Thyroid Cells

Valeria G. Antico Arciuch, Marika A. Russo, Kristy S. Kang, and Antonio Di Cristofano

Abstract

Rapidly proliferating and neoplastically transformed cells generate the energy required to support rapid cell division by increasing glycolysis and decreasing flux through the oxidative phosphorylation (OXPHOS) pathway, usually without alterations in mitochondrial function. In contrast, little is known of the metabolic alterations, if any, which occur in cells harboring mutations that prime their neoplastic transformation. To address this question, we used a *Pten*-deficient mouse model to examine thyroid cells where a mild hyperplasia progresses slowly to follicular thyroid carcinoma. Using this model, we report that constitutive phosphoinositide 3-kinase (PI3K) activation caused by PTEN deficiency in nontransformed thyrocytes results in a global downregulation of Krebs cycle and OXPHOS gene expression, defective mitochondria, reduced respiration, and an enhancement in compensatory glycolysis. We found that this process does not involve any of the pathways classically associated with the Warburg effect. Moreover, this process was independent of proliferation but contributed directly to thyroid hyperplasia. Our findings define a novel metabolic switch to glycolysis driven by PI3K-dependent AMPK inactivation with a consequent repression in the expression of key metabolic transcription regulators. *Cancer Res; 73(17); 5459–72. ©2013 AACR.*

Introduction

Highly proliferative conditions, such as embryonic development, tissue regeneration, lymphocyte activation, and neoplastic transformation, require a complex reorganization of energy metabolism to feed cell growth and division (1). A major feature of this metabolic remodeling is the switch from oxidative phosphorylation (OXPHOS) to aerobic glycolysis, a phenomenon that was first observed by Warburg (2). As a consequence, highly proliferating cells exhibit an increase in the amount of lactate production regardless of oxygen availability (3).

It is widely accepted that several oncogenes, including MYC, hypoxia-inducible factor (HIF)-1α, and AKT (4–6), drive this switch by increasing the expression and activity of glycolytic genes, including hexokinase II, lactate dehydrogenase A, pyruvate kinase M2, and pyruvate dehydrogenase kinase 1 (7–9).

Authors' Affiliation: Department of Developmental and Molecular Biology, Albert Einstein College of Medicine, Bronx, New York

Note: Supplementary data for this article are available at Cancer Research Online (http://cancerres.aacrjournals.org/).

Corresponding Author: Antonio Di Cristofano, Department of Developmental and Molecular Biology, Albert Einstein College of Medicine, Price Center for Genetic and Translational Medicine, 1301 Morris Park Avenue, Room 302, Bronx, NY 10461. Phone: 718-678-1137; Fax: 718-678-1020; E-mail: antonio.dicristofano@einstein.yu.edu

doi: 10.1158/0008-5472.CAN-13-1429

The reduced flux through the tricarboxylic acid (TCA) cycle and OXPHOS is not accompanied by compromised mitochondrial function, and is not associated with alterations in the expression levels of genes involved in oxidative metabolism. One exception to this notion is represented by those tumors in which *FH*, *SDH*, or *IDH* are mutated (10).

To characterize the molecular changes resulting from constitutive activation of the phosphoinositide 3-kinase (PI3K) pathway in tissues where this genetic alteration is causally linked to neoplastic transformation, we have generated a mouse model in which loss of the *Pten* tumor suppressor gene is targeted to the follicular epithelium of the thyroid gland (11). Thyrocyte-specific deletion of *Pten* constitutively activates the PI3K signaling cascade, leading to hyperplastic thyroid glands at birth, to the development of thyroid follicular adenomas by 6 to 8 months of age (11), and of metastatic follicular carcinomas after 1 year of age (12). The progression to neoplastic transformation is dramatically accelerated by simultaneous *Cdkn1b* deletion (12), activation of Kras (13), or *Tp53* deletion (14).

By analyzing the molecular and metabolic alterations found in thyroids from young, tumor-free $Pten^{thyr-/-}$ mice, we have discovered a novel mechanism responsible for the active repression of TCA cycle and OXPHOS in preneoplastic thyrocytes. This pathway is independent of both proliferation and of the known pathways classically associated with the Warburg effect. We show in fact that PI3K activation induces, through the inactivation of AMPK, a coordinated repression of the expression of TCA cycle and respiratory

Published OnlineFirst June 24, 2013; DOI: 10.1158/0008-5472.CAN-13-1429

genes, which favors aerobic glycolysis at the expense of OXPHOS.

Materials and Methods

Animals

The *Pten*$^{L/L}$ and TPO-Cre strains have been previously described (11). *PDK*$^{L/L}$ mice were kindly provided by Dr. Dario Alessi (University of Dundee) (15). All strains were backcrossed in the 129Sv background for at least 10 generations, and littermates were used as controls. RAD001 (Everolimus; kindly provided by Novartis Institutes for Biomedical Research, Basel, Switzerland) was given daily by oral gavage at a dose of 10 mg/kg body weight for 2 weeks, starting at age 4 weeks. 5-Aminoimidazole-4-carboxamide-1-β-4-ribofuranoside (AICAR; TRC) was injected intraperitoneally (i.p.) at 400 mg/kg/d, for 4 weeks, starting at age 4 weeks.

Measurement of glucose uptake by PET

Wild-type (WT) and *Pten*$^{thyr-/-}$ mice were fasted overnight before a tail vein injection of 2[^{18}F]fluoro-2-deoxy-D-glucose (FDG; 300 μCi). One hour after injection, mice were subjected to positron emission tomography (PET) scanning with the Concorde Microsystems R4 microPET Scanner. Animals were imaged while anesthetized by inhalation with isoflurane. Image acquisition was done using the MicroPET Manager with the ASPIRO-dedicated software.

Primary cultures

Thyroid glands were minced and resuspended in Ham's F12/10% FBS with 100 U/mL type I collagenase (Sigma) and 1 U/mL dispase (Roche). Enzymatic digestion was carried out for 90 minutes at 37°C. After digestion, follicles were seeded in Ham's F12 containing 40% Nu-Serum IV (Collaborative Biomedical), gly-his-lys (10 ng/mL; Sigma), and somatostatin (10 ng/mL; Sigma) and allowed to spread for 24 to 36 hours before carrying out the experiments.

Proliferation analysis

Anti-Ki67–stained thyroid sections were photographed at ×400 magnification and analyzed using the ImageJ software. Between 1,500 and 3,000 cells per slide were analyzed. For bromodeoxyuridine (BrdUrd) incorporation experiments, mice were injected i.p. with BrdUrd (10 mg/kg; Sigma) and dissolved in PBS 2 hours before sacrifice. Anti-BrdUrd–stained sections were analyzed as above.

Lactate assay

Lactate levels were assayed using a commercially available kit (Biovision). Lactate levels were normalized to the amount of DNA or proteins extracted from each tissue fragment or primary culture.

Oxygen consumption rate and extracellular acidification rate

Freshly isolated thyroid follicles from pools of 12 WT or 3 mutant mice were plated as described in "Primary cultures," and oxygen consumption rate (OCR) was measured using the Seahorse XF24 instrument (Seahorse Biosciences) under basal conditions, in the presence of the mitochondrial inhibitor oligomycin (1 μg/mL), the mitochondrial uncoupler carbonyl cyanide 4-(trifluoromethoxy)phenylhydrazone (FCCP; 1 μmol/L), and the respiratory chain inhibitors antimycin A (2 mmol/L) and rotenone (0.1 μmol/L).

Flow cytometry analysis of mitochondrial membrane potential

Primary thyroid cells were treated with solvent or 20 μmol/L FCCP for 10 minutes before staining with 100 nmol/L tetramethylrhodamine, ethyl ester (TMRE; Invitrogen) for 20 minutes. Cells were rinsed in Dulbecco's PBS (DPBS), trypsinized, and analyzed for TMRE staining by flow cytometry.

Western blot analysis

Thyroids and cells were homogenized on ice in radioimmunoprecipitation assay (RIPA) buffer supplemented with Complete Protease Inhibitor Tablet (Roche Diagnostics). Western blot analysis was conducted using 20 to 40 μg proteins using antibodies from Cell Signaling Technology, except for aconitase 2, isocitrate dehydrogenase 3a, HIF-1α, and succinate dehydrogenase b (Santa Cruz Biotechnology) and β-actin (Sigma-Aldrich).

Cell lines and drug treatments

FTC-133 cells (kindly donated by Dr. Matthew Ringel, Ohio State University, Columbus, OH) were maintained in Dulbecco's Modified Eagle Medium (DMEM) with 10% FBS at 37°C in 5% CO_2. 8505c cells (kindly donated by Dr. Sareh Parangi, Massachusetts General Hospital, Boston, MA) and THJ16T cells (kindly donated by Dr. John A. Copland, Mayo Clinic, Jacksonville, FL) were grown in RPMI medium with 10% FBS. All cell lines were validated before starting the experiments by amplifying and sequencing genomic fragments encompassing their known mutations (FTC133: *PTEN* R130*,8505c: *BRAF* V600E, THJ16T: *PIK3CA* E545K).

Pharmacologic inhibitors of protein kinase A (PKA; H89; Cell Signaling Technology), and PI3K (BKM120; Selleck Chemicals), or AMP analog (AICAR; TRC) were added 24 hours after plating. After 30 minutes, samples were collected and prepared for Western blot analysis. For luciferase and quantitative PCR (qPCR) experiments, samples were collected after 72 hours.

Real-time PCR

Total RNA was extracted with TRIzol and reverse transcribed using the ThermoScript Kit (Life Technologies). Quantitative real-time PCR (qRT-PCR) was conducted on a StepOne Plus apparatus using the Absolute Blue qPCR Rox Mix (Thermo Scientific) and TaqMan expression assays (Applied Biosystems). Each sample was run in triplicate and *GusB* or *β-actin* was used to control the input RNA. Data analysis was based on the C_t method and experiments were repeated at least three times using at least two independent thyroid pools (at least five mice/pool).

AMP, ADP, ATP level determination

AMP, ADP, and ATP levels were assayed using three independent thyroid pools (10 mice/pool). Approximately, 30 mg of

Published OnlineFirst June 24, 2013; DOI: 10.1158/0008-5472.CAN-13-1429

tissue was extracted in 210 μL of extraction solvent, 40%/40%/20% acetonitrile/methanol/0.1% formamide in water containing a 15N_AMP extraction standard. The column [Sequent ZIC-cHILIC (3.5 μm, 100 mm × 2.1 mm, inner diameter)] was run with a gradient of 90% acetonitrile/10% water containing 10 mmol/L ammonium formate, pH 3.0, at 0.2 mL/min using an ACQUITY ultra performance liquid chromatography attached to a Waters Xevo triple quadruple mass spectrometry.

Transient transfection assays

Cells were transfected with 1 μg PGC-1α WT or T177A/S538A plasmid (#1026, #18093; Addgene). After 24 hours, cells were treated with 1 mmol/L AICAR (TRC) for 48 hours and collected for RNA isolation.

Dual luciferase assay

Cells were cotransfected with 10 ng phRG-TK plasmid (Promega) and 2 μg PGC-1α promoter luciferase plasmid (#8887; Addgene). After 24 hours, cells were treated with inhibitors for 48 hours and collected for dual-luciferase reporter assay (Promega).

Transmission electron microscopy

Thyroid glands were fixed with 2% paraformaldehyde and 2.5% glutaraldehyde in 0.1 mol/L sodium cacodylate buffer, postfixed with 1% osmium tetroxide followed by 1% uranyl acetate, dehydrated through a graded series of ethanol and embedded in LX112 resin (LADD Research Industries). Ultrathin (80 nm) sections were cut on a Reichert Ultracut UCT, stained with uranyl acetate followed by lead citrate, and viewed on a JEOL 1200EX transmission electron microscope at 80 kV.

Proteomic analysis

Sets of thyroid extracts (100 μg) from 3-month-old WT and mutant mice were subjected to two-dimensional (2D) gel electrophoresis (pH 4-11) and Sypro Ruby gel staining as described in ref. 16. About 30 differentially expressed spots were selected for cutting and in-gel tryptic digestion. Matrix-assisted laser desorption/ionization–time-of-flight (MALDI-TOF) peptide mass fingerprinting was conducted as described in ref. 16. Liquid chromatography/tandem mass spectrometry (LC/MS-MS) peptide sequencing was conducted as described in ref. 17. All analyses were conducted by the Fox Chase Cancer Center Proteomics Facility, Philadelphia, PA.

Statistical analysis

Experiments were carried out at least three times. Data were analyzed using the Prism software package. Differences with P values less than 0.05 were considered statistically significant.

Results

Constitutive PI3K activity results in transcriptional repression of TCA cycle and OXPHOS genes

The thyroids of *Pten*$^{thyr-/-}$ mice are enlarged from birth due to an increase in the thyrocytes' proliferative index associated with constitutive PI3K signaling. However, these glands do not display any functional alteration or signs of neoplastic transformation until the mice are at least 10 months of age (12).

To identify early molecular changes that may favor or contribute to the development of thyroid tumors in aging mice, we have initially used a small-scale proteomic approach to detect proteins differentially expressed in thyroids from 3-month-old WT and *Pten*$^{thyr-/-}$ mice. Several spots, with significantly different intensity between normal and mutant thyroids, were selected and excised from 2D gels, and 35 proteins were identified using MALDI-TOF and LC/MS-MS. Surprisingly, 7 of 28 proteins found downregulated in mutant thyroids were enzymes involved in the TCA cycle (Table 1). To validate these findings, we measured by RT-PCR the mRNA levels of the genes encoding these proteins and found that *Cs*, *Aco2*, *Idh3a*, *Dld*, *Pdhb*, and *SdhA* expression in mutant thyroids was reproducibly 20% to 50% lower compared with that of WT glands, whereas the expression of the glucose transporter *Glut1* was slightly increased (Fig. 1A). Downregulation of these genes was also confirmed by Western blot analysis using antibodies specific for aconitase 2, isocitrate dehydrogenase 3a, and succinate dehydrogenase b (Fig. 1B).

To determine to what extent metabolic genes are transcriptionally deregulated upon PI3K activation, we interrogated our Affymetrix gene expression dataset (14) to extend the analysis to all the genes directly involved in the TCA cycle and glycolysis. Interestingly, while none of the glycolytic enzymes was transcriptionally deregulated in the mutant glands (with the exception of a modest increase in the *Glucokinase* mRNA

Table 1. Proteomic identification of differentially regulated TCA cycle enzymes

Swiss-Prot name	Protein name	Expression (WT vs. −/−)	ID method	Score	Coverage	Queries matched
DHSA	Succinate dehydrogenase	2.71	MALDI-TOF	74	16	N/A
IDH3A	Isocitrate dehydrogenase	34.13	MALDI-TOF	71	25	N/A
MDHM	Malate dehydrogenase	2.27	MALDI-TOF	106	30	N/A
ACON	Aconitate hydratase	WT only	LC/MS-MS	382	N/A	15
DLDH	Dihydrolipoyl dehydrogenase	3.22	LC/MS-MS	283	N/A	14
ODPB	Pyruvate dehydrogenase	6.00	LC/MS-MS	150	N/A	6
CISY	Citrate synthase	4.01	LC/MS-MS	132	N/A	9

Abbreviation: N/A, not applicable.

Published OnlineFirst June 24, 2013; DOI: 10.1158/0008-5472.CAN-13-1429

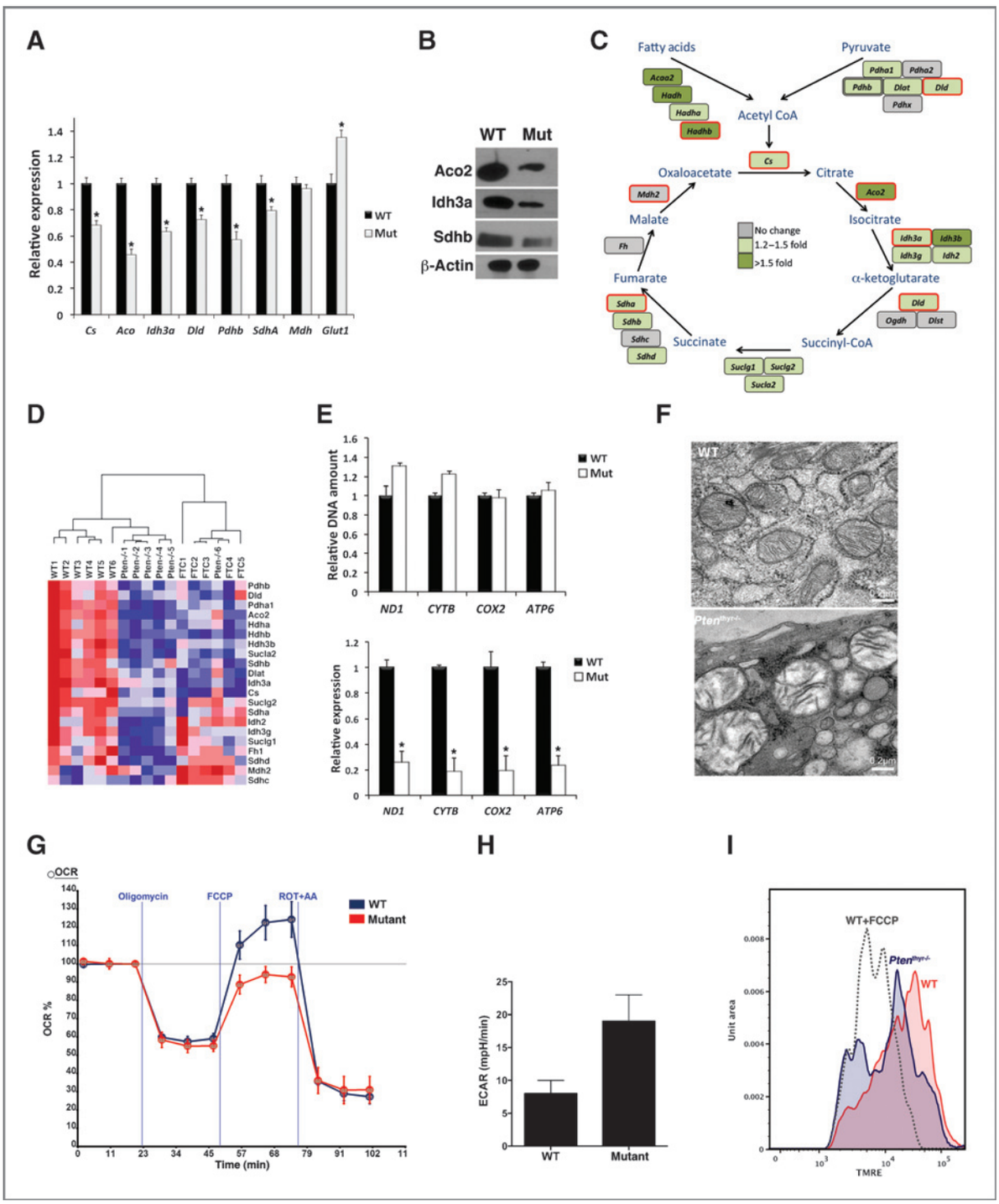

Figure 1. Metabolic reprogramming in *Pten*$^{thyr-/-}$ mice. A, relative expression of the indicated genes in WT and mutant thyroids. Bars represent mean ± SD of triplicate measurements. *, significant ($P < 0.05$) differences. B, Western blot analysis showing downregulation of representative TCA cycle enzymes in mutant glands. C, TCA cycle diagram showing the genes downregulated in *Pten*$^{thyr-/-}$ thyroids. The color scale reflects changes calculated from the Affymetrix data. Genes circled in red have been validated by qPCR. D, heatmap showing the repression of TCA cycle genes in *Pten*$^{thyr-/-}$ thyroids and in follicular carcinomas (FTC) arising in older mice. E, DNA content-based assessment of mitochondria number in 3-month-old WT and mutant mice (top). Expression levels of selected mitochondrial genes in the thyroids of WT and mutant mice (bottom). Bars represent mean ± SD of triplicate measurements. *, significant ($P < 0.05$) differences. F, mitochondrial damage (swelling, clarification, and cristae disruption) in *Pten*$^{-/-}$ glands detected by transmission electron microscopy. G, OCR in control and mutant primary thyrocytes cells in response to 1 μg/mL oligomycin, 1 μmol/L FCCP, or 2 μmol/L antimycin A + 2 μmol/L rotenone. H, ECAR in control and mutant primary thyrocytes cells. $P = 0.004$. I, mitochondrial membrane polarization was measured in primary thyrocytes by flow cytometry using TMRE. FCCP pretreatment of WT cells was used to determine the baseline.

Published OnlineFirst June 24, 2013; DOI: 10.1158/0008-5472.CAN-13-1429

levels), the expression of 22 of 28 genes encoding enzymes associated with the TCA cycle was significantly repressed in *Pten*$^{-/-}$ thyroids (Fig. 1C; data not shown). About 60% of these genes were still repressed in the metastatic follicular carcinomas developing in older *Pten*$^{thyr-/-}$ mice (Fig. 1D).

Furthermore, when we quantitated citrate and isocitrate in the thyroids of control and *Pten*$^{thyr-/-}$ mice by gas chromatography-mass spectroscopy (GC-MS), we found significantly reduced levels of these metabolites in the mutant glands (citrate, 2,577 $\pm$ 525 pmol/mg in the WT and 985 $\pm$ 302 in the mutants; isocitrate, 217 $\pm$ 42 pmol/mg in the WT and 80 $\pm$ 26 in the mutants).

The tight connection existing between TCA cycle, OXPHOS, and mitochondrial fitness prompted us to test whether this global downregulation of TCA cycle genes is accompanied by alterations of the expression of mitochondrial-encoded OXPHOS genes, as well as by changes in the number of mitochondria. We first used RT-PCR to measure the relative mitochondrial genome copy number by amplifying four different mitochondrially encoded genes and one reference nuclear gene from total (genomic and mitochondrial) DNA isolated from WT and mutant thyroids. No significant differences were found between control and mutants, suggesting that constitutive PI3K activation does not alter mitochondrial mass in the mouse thyroid (Fig. 1E). Conversely, the expression of most mitochondrial-encoded genes was heavily downregulated in *Pten*$^{-/-}$ thyroids (Fig. 1E). Furthermore, electron microscopy analysis of control and mutant thyroid sections showed that *Pten* loss caused profound morphologic defects in the mitochondria, including swelling, matrix clarification, and disruption of the cristae (Fig. 1F). All these features are commonly associated with reduced mitochondrial oxidative capacity (18).

To test whether the aforementioned findings reflect an impairment in mitochondrial function, we measured OCR as well as extracellular acidification rate (ECAR) in primary cultures of control and *Pten*$^{-/-}$ thyrocytes. Strikingly, *Pten*$^{-/-}$ thyrocytes exhibited significantly reduced spare respiratory capacity, that is, lower maximal rate of respiration (Fig. 1G) and increased ECAR (Fig. 1H). Finally, we used flow cytometry to compare the mitochondrial membrane potential in primary cultures of control and *Pten*$^{-/-}$ thyrocytes using the cationic potential-sensitive dye, TMRE, which accumulates in intact mitochondria. The main population of mutant cells displayed reduced mitochondrial membrane potential compared with control thyrocytes (about 50% of WT levels, note the logarithmic scale; Fig. 1I), whereas a second population of mutant cells was characterized by even lower potential, similar to that of cells treated with the uncoupler FCCP.

Taken together, these data show that constitutive PI3K activation in the mouse thyroid results in the coordinated downregulation of the expression of genes encoding members of both the TCA cycle and OXPHOS pathways, in extensive mitochondrial damage, and in severe impairment of mitochondrial function.

A glycolytic switch in preneoplastic *Pten*$^{-/-}$ thyrocytes

Because the expression changes described earlier result in reduced efficiency of the TCA cycle/OXPHOS metabolic pathway, the mutant cells might have to increase their glycolytic rate to meet their energetic needs.

As a proxy for the thyrocytes' glycolytic rate, we assessed the amount of lactate present in thyroids from 3-month-old WT and mutant mice. Strikingly, *Pten*$^{-/-}$ thyroids displayed a 3-fold increase in normalized lactate content, suggesting a higher metabolic flux through glycolysis (Fig. 2A). Along the same line, we measured the lactate secretion rate in primary thyrocyte cultures. Mutant cells produced 3- to 5-fold more lactate than their WT counterparts (Fig. 2B), strongly indicating that glycolysis is indeed upregulated to compensate the PI3K-mediated repression of the TCA cycle/OXPHOS pathway. Finally, to validate this hypothesis, we conducted FDG-PET imaging on control and *Pten*$^{thyr-/-}$ mice and found that the hyperplastic *Pten*$^{-/-}$ thyroids showed strong FDG uptake, whereas no uptake was detected in WT mice (Fig. 2C).

These data show that, in response to constitutive PI3K activation, thyroid epithelial cells undergo a glycolytic switch, which is functionally reminiscent of the Warburg effect observed in cancer cells, as well as in highly proliferating cells such as activated lymphocytes.

The Warburg effect is usually driven by a set of "master genes," including *c-MYC*, *AKT*, *mTOR*, and *HIF-1α*, which control the expression, localization, and function of both glucose transporters and glycolytic enzymes (5, 19). Upregulation of hexokinase 2, pyruvate kinase M2, and lactate dehydrogenases A and B are hallmarks of this glycolytic switch.

The establishment of a glycolytic switch in slowly proliferating, non-neoplastic (i.e., nontransformed) cells, and the absence of glycolytic genes upregulation in our expression profiling data would argue against a mechanism involving the classical Warburg effect–related master regulators. In fact, we did not detect significant alterations in the expression levels of *Hif-1α*, *c-Myc*, *Hk2*, *Pkm2*, *Ldha*, or *Ldhb* both at the RNA and protein level (Fig. 2D and E; data not shown).

These data suggest that PI3K activation in nontransformed thyroid epithelial cells induces a glycolytic switch through a novel molecular mechanism.

Pdk1 drives TCA cycle/OXPHOS gene repression downstream of PI3K, independent of mTOR

Pdk1 is an essential member of the PI3K cascade, as it phosphorylates Akt on T308 and S6k1 on T229, allowing their full activation (20). To test to what extent the TCA cycle gene repression observed in *Pten*$^{-/-}$ thyroids depends on the Pdk1/Akt/mTOR cascade, we first crossed *Pten*$^{thyr-/-}$ mice to *Pdk1* conditional mutants (21), obtaining simultaneous thyroid-specific deletion of these two genes. Combined loss of *Pten* and *Pdk1* rescued both the repression of the TCA cycle genes (Fig. 3A) and that of mitochondrially encoded OXPHOS genes (Fig. 3B). Interestingly, mitochondrial DNA (mtDNA)-encoded gene expression in the compound mutants was higher than in WT controls. Furthermore, simultaneous inactivation of *Pten* and *Pdk1* restored lactate production in the thyroid to WT levels (Fig. 3C).

Constitutive PI3K activation in the thyroid follicular cells results in mTOR activation (22), and mTOR activity has been proposed to play a key role in establishing the glycolytic switch

Published OnlineFirst June 24, 2013; DOI: 10.1158/0008-5472.CAN-13-1429

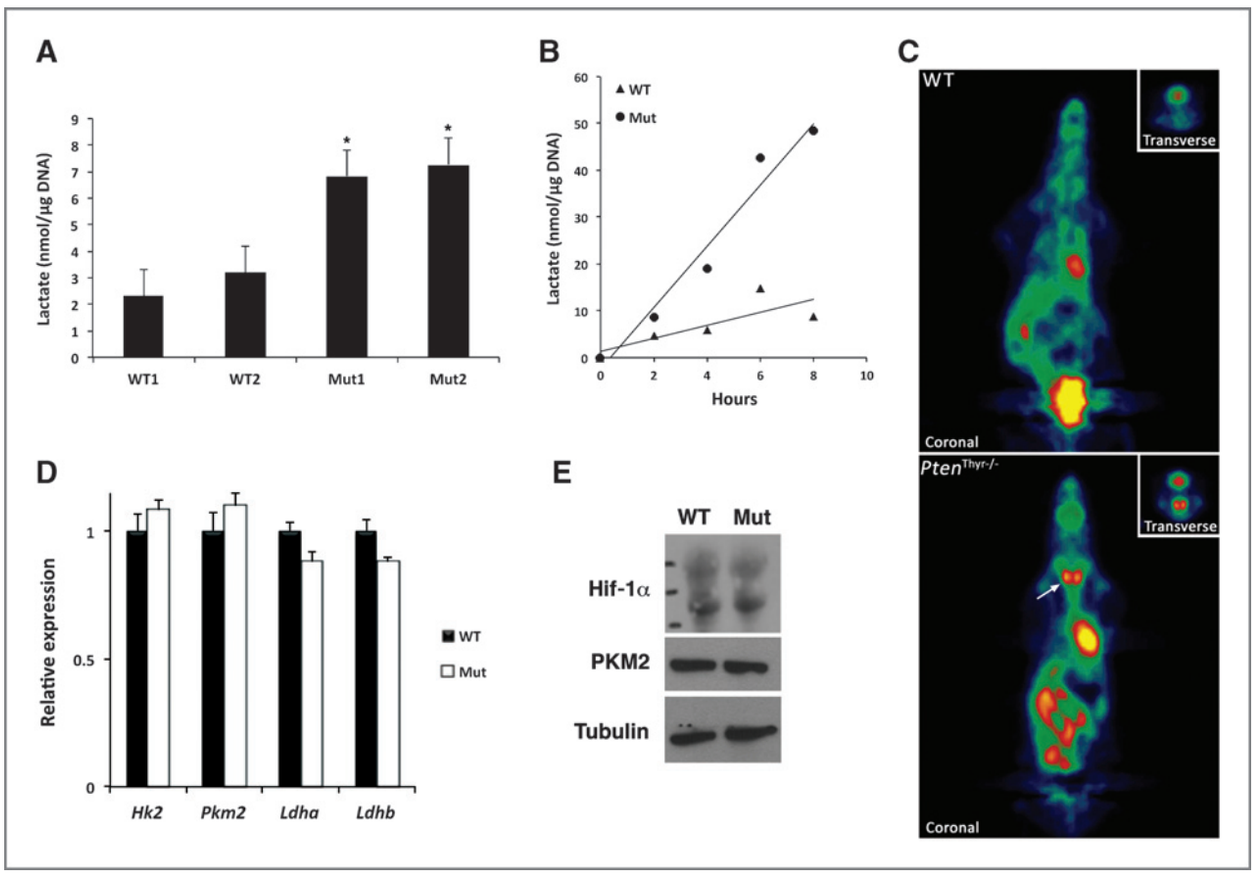

Figure 2. Enhanced glycolysis in *Pten*$^{-/-}$ thyroids. A, lactate levels in the thyroids of 3-month-old WT and mutant mice. Bars represent mean ± SD ($n = 4$/pool). B, lactate production rate in primary cultures of WT and mutant thyrocytes. C, FDG microPET analysis showing increased glucose uptake in 3-month-old mutant mice compared with WT controls. The inset shows a transverse section centered on the thyroid. D, expression levels of the indicated genes in WT and mutant thyroids. Bars represent mean ± SD of triplicate experiments. E, Western blot analysis showing no deregulation of Hif-1α and PKM2 in mutant glands. *, significant ($P < 0.05$) differences.

(23). To test the role of the PI3K/Akt/mTOR axis in the metabolic phenotype of *Pten*$^{thyr-/-}$ mice, we treated 3-month-old WT and mutant mice ($n = 5$/group) daily for 2 weeks with the mTOR inhibitor RAD001 or placebo (Fig. 3D). As previously shown by our group, this treatment is sufficient to inhibit mTOR activity and drastically reduce proliferation in mutant thyroids (Fig. 3D and E; ref. 22). Strikingly, despite the clear inhibition of the thyrocytes' proliferation rate, RAD001 treatment had no effect on the repression of TCA cycle genes (Fig. 3F), on the repression of mitochondrial genes (Fig. 3G), or on thyroid lactate production (Fig. 3H).

These data strongly suggest that PI3K activation in thyroid cells induces a glycolytic switch independent of mTOR activity. Furthermore, they show that the increase in glycolysis in *Pten*$^{thyr-/-}$ mice is not a direct consequence of the increased proliferative rate observed in the hyperplastic glands.

PI3K/AKT inhibit AMPK, leading to decreased OXPHOS metabolism in preneoplastic thyrocytes

The expression of nucleus- and mitochondrial-encoded respiratory proteins is controlled by a number of nucleus-encoded transcription factors and coactivators that modulate mitochondrial function in response to extra- and intracellular signals.

To identify the mechanism through which loss of *Pten* results in a coordinated reprogramming of the expression of respiratory genes, we initially measured in thyroids from 3-month-old WT and *Pten*$^{thyr-/-}$ mice the expression levels of the transcription factors and cofactors involved in the regulation of TCA cycle/OXPHOS. Although the expression levels of *ERRβ*, *PRC*, *NRF-1* and *-2*, and *TFAM* were not altered by constitutive PI3K activation, *Pten*$^{thyr-/-}$ thyroids had significantly lower expression of *ERRγ*, *PGC-1α* and *-β*, and, to a lesser extent, *ERRα* (Fig. 4A). These data suggest that PI3K activation might alter the expression or activity of a common master regulatory gene.

Recently published data have directed our attention on AMPK as a candidate for this role. AMPK contributes to the control of respiratory genes in muscle cells (24) and phosphorylates PGC-1α on T177 and S538 to increase its transcriptional activity, including its ability to transactivate its own promoter (25). In addition, the *ESRRA* promoter contains a PGC-1α/ERRα-responsive regulatory element that can also be

Published OnlineFirst June 24, 2013; DOI: 10.1158/0008-5472.CAN-13-1429

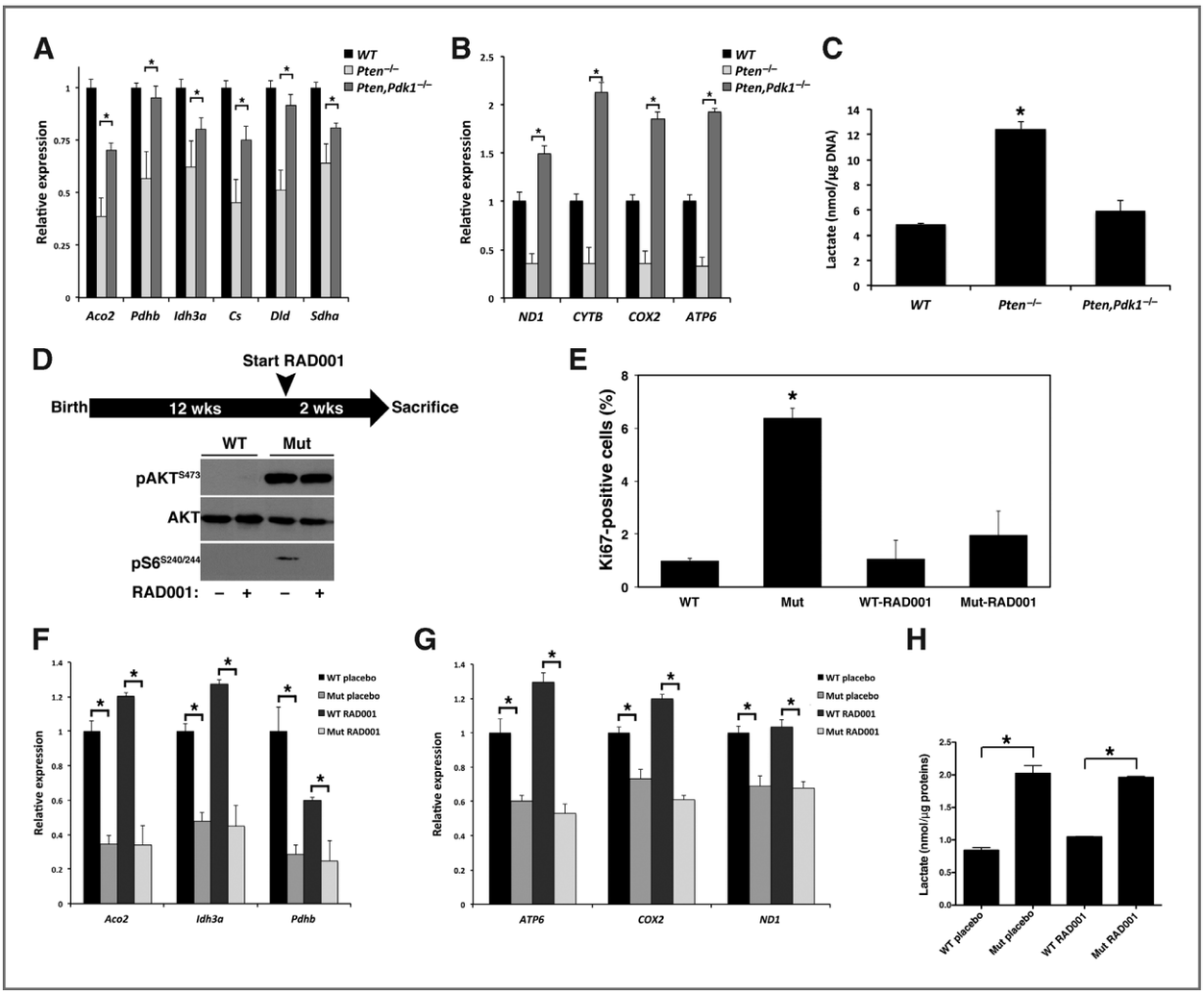

Figure 3. TCA cycle/OXPHOS gene repression depends on Pdk1 but not mTOR. A and B, loss of *Pdk1* restores normal levels of TCA cycle (A) and mitochondrial (B) gene expression in *Pten*$^{thyr-/-}$ mice. Bars represent mean ± SD of triplicate assays. C, loss of *Pdk1* restores normal levels of lactate in *Pten*$^{thyr-/-}$ thyroid glands. Bars represent mean ± SD ($n = 4$/genotype). D, scheme of RAD001 administration to 3-month-old mice and Western blot analysis verification of effective inhibition of mTOR activity. E, mTOR inhibition suppresses thyrocyte proliferation. Bars represent mean ± SD ($n = 5$/genotype). F and G, mTOR inhibition fails to restore normal TCA cycle (F) and mitochondrial (G) gene expression. Bars represent mean ± SD of triplicate assays. H, mTOR inhibition fails to rescue lactate increase in mutant mice. Bars represent mean ± SD ($n = 4$ per genotype). *, significant ($P < 0.05$) differences.

recognized and activated by ERRβ and ERRγ (26). Furthermore, in certain cell types, AKT can phosphorylate AMPK on S485, preventing LKB1 from phosphorylating (on T172) and activating AMPK (27, 28). Indeed, we found that thyroids from *Pten*$^{thyr-/-}$ mice have drastically reduced pT172- and higher pS485-AMPK, compared with WT controls, and reduced levels of phosphorylated ACC (Fig. 4B). Because it is theoretically possible that the reduced levels of pT172-AMPK in the mutant glands might be due to a low AMP/ATP ratio, we measured AMP, ADP, and ATP levels in extracts from WT and mutant glands. AMP and ATP levels in mutant glands were comparable with WT controls, whereas ADP levels were slightly higher on the mutant glands. These data indicate that PI3K inhibits AMPK despite AMP/ATP and ADP/ATP ratios that would stimulate AMPK activation, as in WT glands (Fig. 4C).

To test the hypothesis that PI3K activation represses TCA cycle/OXPHOS gene expression through the inhibition of AMPK, we treated WT and *Pten*$^{thyr-/-}$ mice with the AMPK activator AICAR for 4 weeks, and then isolated their thyroid glands. AICAR treatment increased pT172-AMPK levels not only in WT mice, but also (and to the same levels) in *Pten*$^{thyr-/-}$ mice, despite the persistent AKT activation and inhibitory AMPK phosphorylation on S485 (Fig. 5A). Furthermore, AICAR-activated AMPK restored ACC phosphorylation on Ser79 (Fig. 5D).

We next measured the expression of *ERRα*, *ERRγ*, *PGC-1α*, and *PGC-1β* in the thyroids of control, mutant, and AICAR-treated mutant mice. Strikingly, AICAR treatment increased the mRNA levels of all four transcription factors and cofactors to near-WT levels (Fig. 5B). To verify that the increase in transcriptional regulator levels translates in a restoration

Published OnlineFirst June 24, 2013; DOI: 10.1158/0008-5472.CAN-13-1429

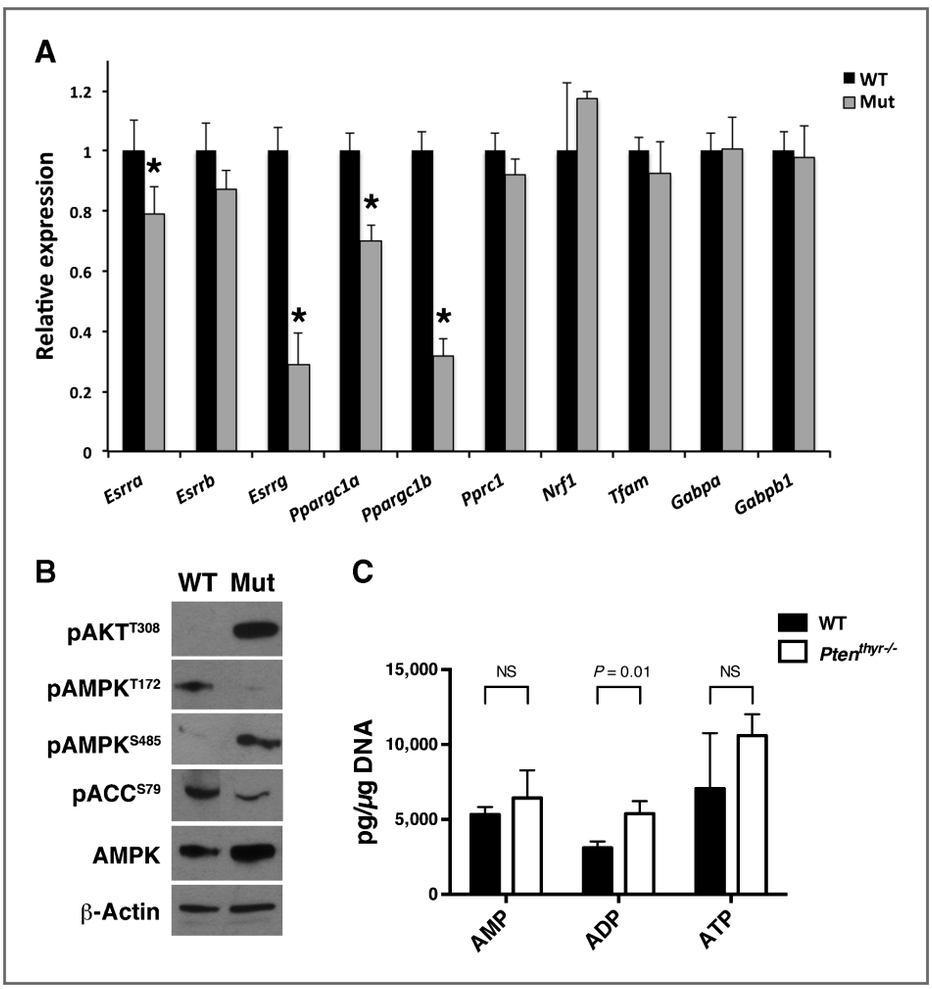

Figure 4. AMPK is repressed in *Pten*$^{thyr-/-}$ thyroids. A, qPCR profiling of metabolic transcriptional regulators in the thyroids of control and mutant mice. Bars represent mean ± SD of triplicate assays. *, significant ($P < 0.05$) differences. B, Western blot analysis of AMPK activation in WT and mutant glands. C, AMP, ADP, and ATP levels in thyroids from WT and *Pten*$^{thyr-/-}$ mice. Bars represent mean ± SD ($n = 3$ pools of 10 thyroids per genotype). NS, not significant.

of normal TCA cycle/OXPHOS gene expression, we measured by qPCR and Western blotting the expression levels of selected TCA cycle genes, and found that AICAR treatment had completely rescued the PI3K-dependent repression of *Aco2*, *Idh3a*, and *Pdhb* (Fig. 5C and D). However, when we tested the expression of the mitochondrial-encoded OXPHOS genes, we could only detect a partial rescue upon AICAR treatment (Fig. 5E). Furthermore, the extent of mitochondrial damage observed in *Pten*$^{thyr-/-}$ thyrocytes was only mildly reduced by AICAR treatment (Fig. 5F). Despite the persistence of some mitochondrial damage, enforced AMPK activation reversed the glycolytic switch induced by constitutive PI3K activation, as shown by the reduction of lactate content to WT levels in AICAR-treated *Pten*$^{thyr-/-}$ mice (Fig. 5G).

These data strongly suggest that PI3K/AKT–mediated AMPK inhibition is responsible for the repression of oxidative metabolism gene expression observed in *Pten*$^{thyr-/-}$ mice.

AMPK inhibition actively contributes to thyroid hyperplasia

To test whether the glycolytic switch observed in *Pten*$^{thyr-/-}$ mice plays an active role in the hyperproliferative and protumorigenic phenotype of mutant thyrocytes, we compared the weight and proliferative index of WT, *Pten*$^{thyr-/-}$, and AICAR-treated mutant thyroid glands. During the 4 weeks of enforced AMPK reactivation, mutant glands grew at a much slower rate compared with untreated mutants, so that the weight of the mutant thyroids at the end of the treatment was significantly reduced compared with untreated *Pten*$^{thyr-/-}$ mice (−34%; Fig. 5H). This size reduction was associated with decreased proliferation: the thyrocyte proliferation index in AICAR-treated mice, determined by BrdUrd incorporation, was drastically reduced, compared with that of untreated mutant mice (−53%; Fig. 5I). Thus, it is possible that that the glycolytic switch caused by PI3K-mediated AMPK inhibition actively contributes to the development of thyroid hyperplasia in *Pten*$^{thyr-/-}$ mice.

The PI3K/AMPK–mediated repression of oxidative metabolism is maintained in human thyroid cancer cells and involves AMPK-mediated phosphorylation of PGC-1α

Having established in a relevant *in vivo* system that sustained PI3K activation redirects energy metabolism toward glycolysis by repressing the expression of TCA cycle

Published OnlineFirst June 24, 2013; DOI: 10.1158/0008-5472.CAN-13-1429

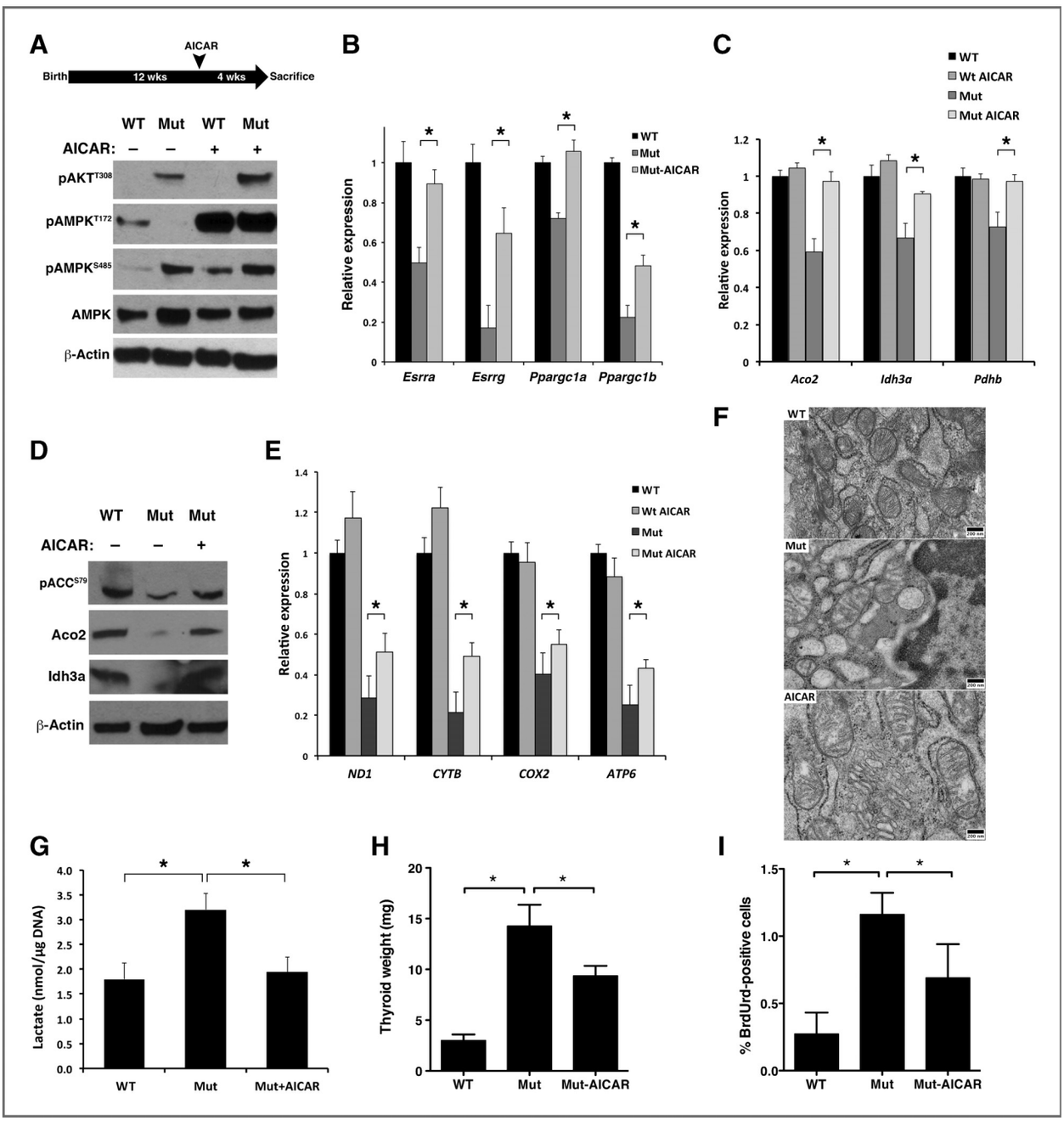

Figure 5. AICAR-mediated AMPK activation reverts the metabolic switch in *Pten*$^{thyr-/-}$ thyroids. A, top, scheme of AICAR administration: 3-month-old mice were injected intraperitoneally with AICAR (400 mg/kg/d) for 4 weeks. Bottom, Western blot analysis of the effect of *in vivo* AICAR treatment on the phosphorylation of AMPK. B and C, expression levels of selected metabolic transcriptional regulators (B) and TCA cycle genes (C) upon *in vivo* AICAR treatment. Bars represent mean ± SD of triplicate assays. D, Western blotting showing that *in vivo* AICAR treatment rescues TCA cycle enzymes expression. E, expression levels of mitochondrial genes in the thyroids of control and AICAR-treated mice. Bars represent mean ± SD of triplicate assays. F, transmission electron microscopy showing mitochondria structure in the thyroids of WT, *Pten*$^{-/-}$, and AICAR-treated *Pten*$^{-/-}$ mice. G, effect of the *in vivo* AICAR treatment on lactate production. Bars represent mean ± SD ($n = 4$/genotype). H, thyroid weight in WT, mutant, and AICAR-treated mutant mice. I, proliferation index of thyroids from WT, mutant, and AICAR-treated mutant mice as measured by BrdUrd incorporation. *, significant ($P < 0.05$) differences.

and OXPHOS genes in mouse thyrocytes, we sought to extend these studies to the human setting. We have initially used the *PTEN*$^{-/-}$ follicular thyroid cancer cell line, FTC-133, untreated, normally growing cells displayed almost undetectable pT172-AMPK, and strong pS485-AMPK. In keeping with the mouse data, AICAR treatment increased pT172-AMPK, as well as pS79-ACC (a direct AMPK target) in a dose-dependent manner (Fig. 6A). Furthermore, enforced

Published OnlineFirst June 24, 2013; DOI: 10.1158/0008-5472.CAN-13-1429

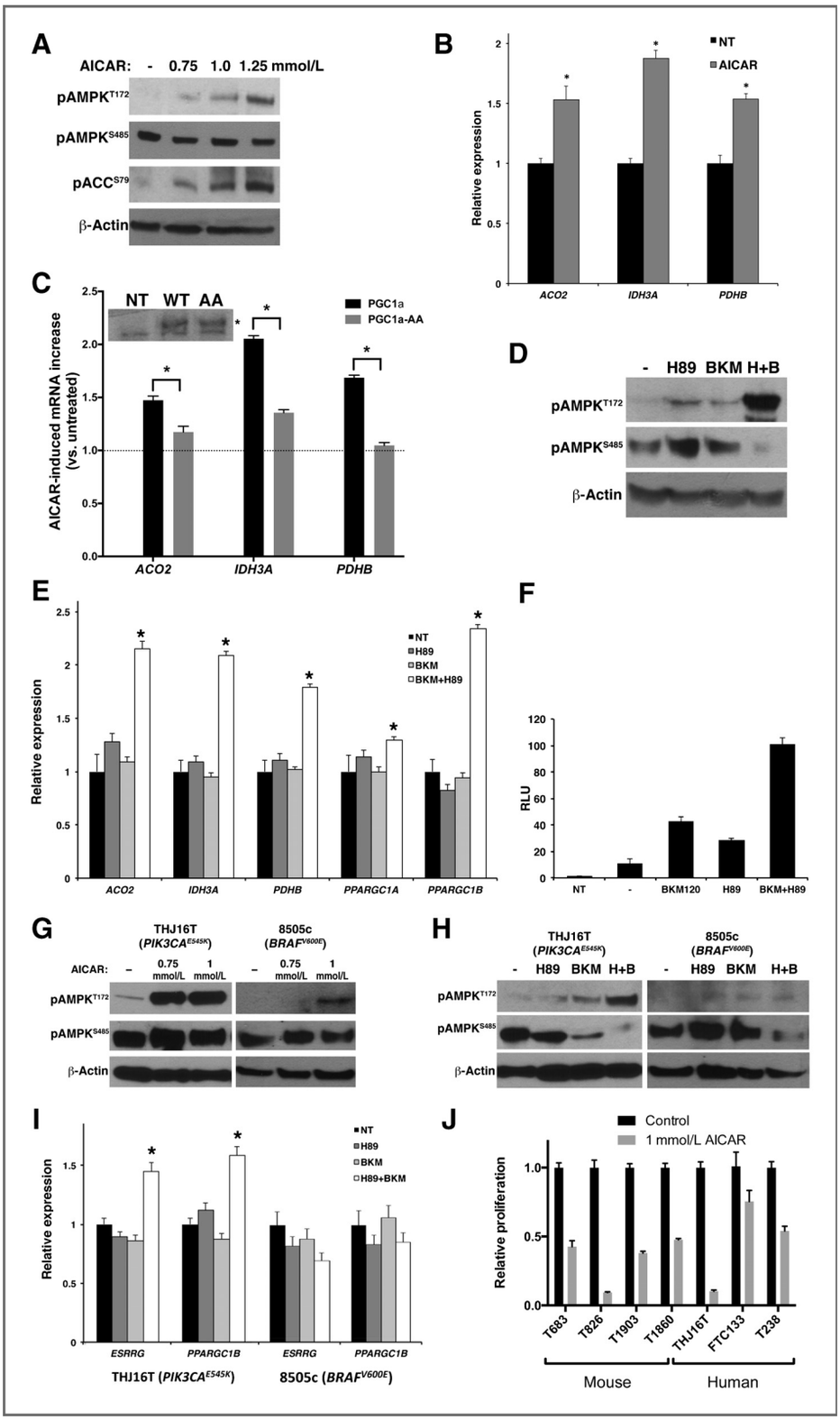

Figure 6. The AKT/AMPK/PGC-1α/TCA cycle axis is conserved in human thyroid cancer cells. A, Western blot analysis of the effect of AICAR treatment on AMPK phosphorylation status in FTC-133 cells. B, expression analysis of representative TCA cycle genes in FTC-133 cells upon AICAR treatment. Bars represent mean ± SD of triplicate assays. C, AICAR-induced increase in the expression levels of representative TCA cycle genes in FTC-133 cells transfected with WT or mutant (AA) PGC-1α. Top, Western blot analysis showing comparable expression levels of transfected WT and mutant (AA) PGC-1α (specific band marked with an *). D, Western blot analysis of the effect of H89, BKM120, and their combination on AMPK phosphorylation in FTC-133 cells. E, expression levels of representative metabolic transcriptional regulators and TCA cycle genes upon H89, BKM120, and their combination treatment in FTC-133 cells. Bars represent mean ± SD of triplicate assays. F, luciferase assay showing PGC-1α promoter activity in FTC-133 cells after treatment with the indicated inhibitors. Bars represent mean ± SD ($n = 3$/treatment). RLU, relative luciferase units. G, Western blot analysis of the effect of AICAR treatment of THJ16T and 8505c cells on AMPK phosphorylation status. H, Western blot analysis of the effect of H89, BKM120, and their combination on AMPK phosphorylation status in THJ16T and 8505c cells. I, expression levels of the *ESRRG* and *PPARGC1B* metabolic transcriptional regulators upon H89, BKM120, and their combination treatment in THJ16T and 8505c cells. Bars represent mean ± SD of triplicate assays. *, significant ($P < 0.05$) differences. J, proliferation of mouse and human thyroid cancer cells treated with 1 mmol/L AICAR and counted after 72 hours. Bars represent mean ± SD of triplicate assays.

reactivation of AMPK led to significantly increased expression of the TCA cycle genes *ACO2*, *IDH3A*, and *PDHB* (Fig. 6B).

As mentioned earlier, AMPK might control the expression and function of metabolic transcription factors and enzymes by modulating PGC-1α activity via phosphorylation on PGC-

Published OnlineFirst June 24, 2013; DOI: 10.1158/0008-5472.CAN-13-1429

1α T177 and S538 (25). To test whether this pathway, discovered in skeletal muscle cells, is also active in thyrocytes, we transfected FTC-133 cells with an expression vector encoding WT or phosphorylation-defective PGC-1α (PGC-1α-AA), treated the cells with vehicle or AICAR to reverse the inhibition of AMPK, and extracted mRNA to measure the expression of a group of TCA cycle genes. AMPK reactivation increased the expression of *ACO2*, *IDH3A*, and *PDHB* in cells transfected with WT PGC-1α but not, or to a much lower extent, in those cells transfected with the PGC-1α- mutant that cannot be phosphorylated (Fig. 6C). Thus, PGC-1α acts as a conduit for AMPK to control the expression of metabolic genes.

To test whether AMPK repression in human cells is directly associated with PI3K activation, we treated FTC-133 cells with the pan-PI3K inhibitor BKM120. Surprisingly, PI3K inhibition at a BKM concentration that has no off-target effects (1 μmol/L) was not sufficient to abolish S485 phosphorylation, or to induce T172 phosphorylation (Fig. 6D). However, higher BKM120 concentrations could achieve these effects (data not shown) suggesting that other related kinases might contribute to S485 phosphorylation and AMPK inhibition.

PKA has been shown to phosphorylate S485-AMPK in the insulin-secreting cell line, INS-1 (29). Furthermore, in mouse adipocytes, PKA can phosphorylate AMPK on S173, inhibiting T172 phosphorylation, likely through steric hindrance (30). Thus, we tested whether PKA inhibition could synergize with PI3K inhibition to restore AMPK activity and respiratory gene expression. Strikingly, while FTC-133 treatment with the PKA inhibitor H89 alone did not result in alterations of the phosphorylation status of AMPK, simultaneous inhibition of PI3K and PKA abolished pS485-AMPK and drastically increased pT172-AMPK (Fig. 6D). Accordingly, while single-inhibitor treatment of FTC-133 failed to increase the expression of TCA cycle genes, or PGC-1α and PGC-1β, combined treatment significantly increased their mRNA levels (Fig. 6E). Combined inhibition of PI3K and PKA was also more effective than either kinase inhibition in increasing the expression of a luciferase reporter driven by the promoter region of *PGC-1α*, further supporting the role of AMPK in the control of PGC-1α activity and expression (Fig. 6F).

These data suggest that the PI3K/AKT axis controls AMPK activity also in $PTEN^{-/-}$ human thyroid cancer cells; however, in these cells, PKA contributes to the metabolic reprogramming through an overlapping pathway.

To test whether this signaling cascade is also active in human anaplastic thyroid cancer, we used two cell lines representative of the most common driver pathways in this aggressive and genetically complex tumor type: THJ16T, harboring an activating *PIK3CA* mutation (E545K), and 8505c, harboring the *BRAF* oncogenic allele V600E.

Both cell lines displayed low to undetectable pT172-AMPK, as well as strong pS485-AMPK, suggesting that AMPK inhibition is a common theme in thyroid cancer (Fig. 6G). AICAR treatment restored T172 phosphorylation, more effectively in the cell line harboring the PI3K oncogenic mutation (Fig. 6G).

When we treated these cells with PI3K and PKA inhibitors, alone and in combination, we found that simultaneous PI3K and PKA inhibition effectively reactivated AMPK and increased the expression of metabolic regulators such as *ERRγ* and *PGC-1β* in cells with constitutively active PI3K; however, they did not affect AMPK activation or *ERRγ* and *PGC-1β* expression in the $BRAF^{V600E}$ cell line (Fig. 6H and I). Similar to the *in vivo* model, AMPK reactivation reduced proliferation of a panel of mouse and human thyroid cancer cell lines carrying PI3K-activating mutations (Fig. 6J).

Thus, in well-differentiated and undifferentiated human thyroid cancer cells, constitutive activation of PI3K, in cooperation with PKA, alters the expression of genes involved in respiratory metabolism by inhibiting AMPK.

TCA cycle gene repression in neoplastic lesions is also observed in other human tissues

To extend our findings to human tumors other than those arising in the thyroid, we interrogated the Oncomine database for datasets showing significant simultaneous downregulation of both *PTEN* and TCA cycle genes. Although this approach does not account for other, more common, PI3K-activating mechanisms, it represents the only direct way to identify, within large expression datasets, tumors with activated PI3K signaling, in the absence of validated "PI3K activation" signatures.

Considering the inherent low power of our search, it is remarkable that we found a very strong association between *PTEN* loss and TCA cycle repression in two datasets, derived from dedifferentiated liposarcoma and from early-stage colon cancer (Supplementary Fig. S1). Thus, other human tumor types display global downregulation of TCA cycle genes in association with *PTEN* loss and PI3K activation, warranting future studies to experimentally validate this association.

Discussion

The existence of a tight link between PI3K signaling and rerouting of energy metabolism is well established in cancer cells, where activation of PI3K contributes to the switch from oxidative to glycolytic pathways through several of its downstream effectors, including AKT, mTOR, and HIF-1α (31). In turn, these effectors increase the expression and/or activity of a variety of glycolytic enzymes, such as hexokinase II (32), phosphofructokinase 2 (33), the GLUT family of glucose transporters (34), lactate dehydrogenases (35, 36), and the M2 isoform of pyruvate kinase (23). Thus, in fully transformed cells, the Warburg effect is achieved through an increase in glycolytic flux, whereas mitochondrial metabolism is unaffected.

Little is known of the mechanism(s) regulating energy metabolism in normal and preneoplastic (i.e., carrying single mutations and not yet transformed) cells. There is a consensus that in normal cells the glycolytic switch is linked to high proliferation rates, as shown for embryonic tissues and activated lymphocytes (37). Although an elegant study has recently established that activated lymphocytes rely mainly on MYC to transcriptionally reprogram their metabolism (38), much less is known when it comes to epithelial cells.

Our data, generated in a relevant *in vivo* model, support the hypothesis that, in response to PI3K activation, nontransformed thyroid epithelial cells increase metabolic flux through

Published OnlineFirst June 24, 2013; DOI: 10.1158/0008-5472.CAN-13-1429

glycolysis, as indicated by the dramatic increase in lactate production observed in mutant cells; however, this metabolic switch is independent of thyrocyte proliferation. Metabolic reprogramming of thyroid epithelial cells is achieved through a previously unknown mechanism, involving the coordinated downregulation of the expression of TCA cycle and OXPHOS genes, and leading to dysfunctional mitochondria and reduced ability to conduct respiratory metabolism. Although we did not observe any significant increase in the expression of glycolytic genes (with the exception of *Glk*) upon *Pten* loss, we found a reproducible upregulation of the *Glut1* transporter. Accordingly, a strong connection between loss of PTEN expression and increased expression of GLUT1 has been recently reported in thyroid tumors discovered during unrelated FDG-PET scans (39).

Our data are in partial agreement with those recently reported by Garcia-Cao and colleagues using a mouse model with enforced whole-body overexpression of *Pten* (40). Mouse embryonic fibroblasts (MEF) from these mice display a metabolic shift toward OXPHOS, decreased lactate production, and increased expression of PGC-1α-target genes. However, in striking contrast with our model, cells overexpressing *Pten* have increased mitochondria number and upregulate *PKM2* through mTOR. Although these differences might be linked to tissue-specificity of some of the controlling pathways, they might also be the consequence of overexpressing Pten, which completely abolishes PI3K signaling. Notably, the expression of OXPHOS genes in *Pten*,*Pdk1*$^{thyr-/-}$ mice (in which PI3K signaling is drastically repressed, like in the *Pten* transgenic strain) was higher than in WT control, supporting the latter hypothesis.

From a mechanistic standpoint, our data support a model in which PI3K activation initiates the remodeling of energy metabolism through the phosphorylation of AMPK on S485 and its consequent inactivation. AMPK is a kinase known to play critical roles in growth, metabolism, autophagy, and cell polarity (41, 42). Its activation requires phosphorylation on T172 by LKB1 (41). Such phosphorylation can be inhibited by the AKT- and PKA-mediated phosphorylation of S485 (29, 43) and by PKA-mediated phosphorylation of S173 (30). A recent report has shown that also S6K1 can inhibit AMPK by phosphorylating S485 (44). However, the fact that RAD001 treatment of mutant mice does not rescue any of the metabolic phenotypes despite the complete ablation of S6K activity argues against a role for S6K1 in the phosphorylation of AMPK, at least in the thyroid. For the same reason, although mTOR was found to be central to the glycolytic switch in *Tsc2*$^{-/-}$ mouse kidney tumors and in *Pten*$^{-/-}$ MEFs (23), our *in vivo* data clearly show that mTOR activation is dispensable for the metabolic remodeling of the preneoplastic thyroid.

AMPK has been recently shown to suppress the Warburg effect in Myc-driven lymphomas, and its genetic inactivation induces a glycolytic shift in MEFs via normoxic stabilization of HIF-1α (45). Conversely, we do not detect changes in HIF-1α protein levels in the thyroids of *Pten*$^{thyr-/-}$ mice, nor upregulation of *Ldha* or *Aldoa*. More importantly, acute AMPK ablation did not affect OCR in both lymphomas and MEFs, suggesting the absence of any detrimental effects on the TCA cycle. These differences with our model might be related to the complete loss of AMPK versus its decreased phosphorylation, or reflect tissue-specific wiring of the metabolic pathways.

ERRs and PGC-1 are major regulators of the expression of TCA cycle/OXPHOS genes, and their loss or overexpression have been shown to lead to repression or induction of these metabolic targets, respectively (24, 46, 47).

Inactivation of AMPK by AKT results in its inability to transactivate PGC-1α (25), which in turn leads to lower levels of ERRα (26). Less clear, instead, is how AMPK controls the expression of PGC-1β, which lacks the two residues phosphorylated by AMPK in PGC-1α, and that of ERRγ. Although ERRγ downregulation might be directly responsible for the reduced levels of PGC-1β (24), its link to PI3K and AMPK is still unclear. It has been recently reported that ERBB2 upregulates (likely through PI3K) microRNA (miR)-378* expression in breast cancer cells (48). In turn, miR-378* targets *ERRγ*, leading to downregulation of TCA cycle genes, reduced respiration rate, and increased glycolysis. Future studies will evaluate whether PI3K activation in thyroid cells targets *ERRγ* through miR-378*, and whether AMPK plays a role in this pathway.

The fact that AICAR treatment rescued only partially the expression of mtDNA-encoded genes and the altered mitochondria morphology in *Pten*$^{thyr-/-}$ mice might be a consequence of the extensive damage sustained by these organelles. Alternatively, additional PI3K-driven pathways might contribute to this aspect of the phenotype. An additional still open question is why PKA affects AMPK activity in thyroid cancer cell lines, but does not seem to do so *in vivo*, in mouse thyrocytes. Further work will be needed to clarify these issues.

One important aspect of our findings is that the metabolic remodeling seems to contribute directly to the hyperproliferative phenotype, as AICAR-mediated restoration of normal levels of TCA cycle enzymes and reduction of glycolytic rate *in vivo* drastically reduces thyrocyte proliferation. However, we cannot completely exclude that the reduced proliferation in AICAR-treated mice is also the consequence of an energy-deprived status due to persistent mitochondrial damage and dysfunction in conditions (i.e., AICAR treatment) that decrease the metabolic flux through glycolysis.

It is tempting to propose that the noncanonical glycolytic switch that takes place in preneoplastic *PTEN*$^{-/-}$ cells might contribute to the neoplastic transformation of thyroid, breast, and colon epithelial cells in patients with Cowden Disease, carrying germline *PTEN* mutations. Similar to *SDHB* or *SDHD* mutation carriers, patients with *PTEN*-mutant Cowden Disease have recently been found to have elevated plasma succinate (49). The downregulation of succinate dehydrogenases expression observed in the thyroids of *Pten*-mutant mice also results in increased succinate levels (Antico and colleagues, manuscript in preparation). A similar protransforming contribution might also take place in endometrial epithelial cells in sporadic type I (endometrioid) endometrial cancer, where loss of PTEN is the earliest recognized genetic alteration (50).

Because the analysis of early hyperplastic lesions with PI3K activation in human tissues is not easily feasible, and relevant expression datasets are not publicly available, to extend our

Published OnlineFirst June 24, 2013; DOI: 10.1158/0008-5472.CAN-13-1429

model to additional human tissues, we used the Oncomine database, and found several datasets in which *PTEN* down-regulation coexists with global repression of TCA cycle genes. Interestingly, one of these datasets is derived from early-stage colorectal cancer (51), supporting our hypothesis that these metabolic changes may take place well before full neoplastic transformation. Finally, a recent proteomic and metabolomic study of gastric cancer, a tumor type often associated with PI3K activation, found extensive repression of TCA cycle genes (52).

In conclusion, our characterization of an *in vivo* model of PI3K activation in thyroid epithelial cells has led to the discovery of a novel pathway, in which the glycolytic switch is not achieved through direct upregulation of glycolytic enzyme expression and activity, but rather through the active inhibition of AMPK and the consequent repression of the expression of TCA cycle and OXPHOS genes, leading to the impairment of mitochondrial metabolism.

Disclosure of Potential Conflicts of Interest

No potential conflicts of interest were disclosed.

Authors' Contributions

Conception and design: V.G.A. Arciuch, A. Di Cristofano
Development of methodology: V.G.A. Arciuch, A. Di Cristofano
Acquisition of data (provided animals, acquired and managed patients, provided facilities, etc.): V.G.A. Arciuch, M.A. Russo, A. Di Cristofano
Analysis and interpretation of data (e.g., statistical analysis, biostatistics, computational analysis): V.G.A. Arciuch, K.S. Kang, A. Di Cristofano
Writing, review, and/or revision of the manuscript: V.G.A. Arciuch, M.A. Russo, K.S. Kang, A. Di Cristofano
Administrative, technical, or material support (i.e., reporting or organizing data, constructing databases): V.G.A. Arciuch, K.S. Kang
Study supervision: V.G.A. Arciuch, A. Di Cristofano

Grant Support

This work was supported by the Albert Einstein Cancer Center Core Grant, and by NIH grants to A. Di Cristofano (CA128943 and CA167839). A. Di Cristofano is a recipient of the Irma T. Hirschl Career Scientist Award. ATP, ADP, and AMP LC/MS assays were established in the Stable Isotope and Metabolomics Core of the Diabetes Research and Training Center (DRTC), supported by NIH grant P60DK020541.

The costs of publication of this article were defrayed in part by the payment of page charges. This article must therefore be hereby marked *advertisement* in accordance with 18 U.S.C. Section 1734 solely to indicate this fact.

Received May 16, 2013; revised June 17, 2013; accepted June 19, 2013; published OnlineFirst June 24, 2013.

References

1. Fritz V, Fajas L. Metabolism and proliferation share common regulatory pathways in cancer cells. Oncogene 2010;29:4369–77.
2. Warburg O. On the origin of cancer cells. Science 1956;123:309–14.
3. Ortega AD, Sanchez-Arago M, Giner-Sanchez D, Sanchez-Cenizo L, Willers I, Cuezva JM. Glucose avidity of carcinomas. Cancer Lett 2009;276:125–35.
4. Elstrom RL, Bauer DE, Buzzai M, Karnauskas R, Harris MH, Plas DR, et al. Akt stimulates aerobic glycolysis in cancer cells. Cancer Res 2004;64:3892–9.
5. Levine AJ, Puzio-Kuter AM. The control of the metabolic switch in cancers by oncogenes and tumor suppressor genes. Science 2010;330:1340–4.
6. Duvel K, Yecies JL, Menon S, Raman P, Lipovsky AI, Souza AL, et al. Activation of a metabolic gene regulatory network downstream of mTOR complex 1. Mol Cell 2010;39:171–83.
7. Qing G, Skuli N, Mayes PA, Pawel B, Martinez D, Maris JM, et al. Combinatorial regulation of neuroblastoma tumor progression by N-Myc and hypoxia inducible factor HIF-1alpha. Cancer Res 2010;70:10351–61.
8. Koppenol WH, Bounds PL, Dang CV. Otto Warburg's contributions to current concepts of cancer metabolism. Nat Rev Cancer 2011;11:325–37.
9. Israel M, Schwartz L. The metabolic advantage of tumor cells. Mol Cancer 2011;10:70.
10. Raimundo N, Baysal BE, Shadel GS. Revisiting the TCA cycle: signaling to tumor formation. Trends Mol Med 2011;17:641–9.
11. Yeager N, Klein-Szanto A, Kimura S, Di Cristofano A. Pten loss in the mouse thyroid causes goiter and follicular adenomas: insights into thyroid function and Cowden disease pathogenesis. Cancer Res 2007;67:959–66.
12. Antico-Arciuch VG, Dima M, Liao XH, Refetoff S, Di Cristofano A. Cross-talk between PI3K and estrogen in the mouse thyroid predisposes to the development of follicular carcinomas with a higher incidence in females. Oncogene 2010;29:5678–86.
13. Miller KA, Yeager N, Baker K, Liao XH, Refetoff S, Di Cristofano A. Oncogenic Kras requires simultaneous PI3K signaling to induce ERK activation and transform thyroid epithelial cells *in vivo*. Cancer Res 2009;69:3689–94.
14. Antico Arciuch VG, Russo M, Dima M, Kang KS, Dasrath F, Liao XH, et al. Thyrocyte-specific inactivation of p53 and Pten results in anaplastic thyroid carcinomas faithfully recapitulating human tumors. Oncotarget 2011;2:1109–26.
15. Lawlor MA, Mora A, Ashby PR, Williams MR, Murray-Tait V, Malone L, et al. Essential role of PDK1 in regulating cell size and development in mice. EMBO J 2002;21:3728–38.
16. Patel BB, Li XM, Dixon MP, Blagoi EL, Seeholzer SH, Chen Y, et al. Searchable high-resolution 2D gel proteome of the human colon crypt. J Proteome Res 2007;6:2232–8.
17. Ke E, Patel BB, Liu T, Li XM, Haluszka O, Hoffman JP, et al. Proteomic analyses of pancreatic cyst fluids. Pancreas 2009;38:e33–42.
18. Bonnard C, Durand A, Peyrol S, Chanseaume E, Chauvin MA, Morio B, et al. Mitochondrial dysfunction results from oxidative stress in the skeletal muscle of diet-induced insulin-resistant mice. J Clin Invest 2008;118:789–800.
19. Cairns RA, Harris IS, Mak TW. Regulation of cancer cell metabolism. Nat Rev 2011;11:85–95.
20. Pearce LR, Komander D, Alessi DR. The nuts and bolts of AGC protein kinases. Nat Rev Mol Cell Biol 2010;11:9–22.
21. Bayascas JR, Sakamoto K, Armit L, Arthur JS, Alessi DR. Evaluation of approaches to generation of tissue-specific knock-in mice. J Biol Chem 2006;281:28772–81.
22. Yeager N, Brewer C, Cai KQ, Xu XX, Di Cristofano A. Mammalian target of rapamycin is the key effector of phosphatidylinositol-3-OH-initiated proliferative signals in the thyroid follicular epithelium. Cancer Res 2008;68:444–9.
23. Sun Q, Chen X, Ma J, Peng H, Wang F, Zha X, et al. Mammalian target of rapamycin up-regulation of pyruvate kinase isoenzyme type M2 is critical for aerobic glycolysis and tumor growth. Proc Natl Acad Sci U S A 2011;108:4129–34.
24. Narkar VA, Fan W, Downes M, Yu RT, Jonker JW, Alaynick WA, et al. Exercise and PGC-1alpha-independent synchronization of type I muscle metabolism and vasculature by ERRgamma. Cell Metab 2011;13:283–93.
25. Jager S, Handschin C, St-Pierre J, Spiegelman BM. AMP-activated protein kinase (AMPK) action in skeletal muscle via direct phosphorylation of PGC-1alpha. Proc Natl Acad Sci U S A 2007;104:12017–22.
26. Giguere V. Transcriptional control of energy homeostasis by the estrogen-related receptors. Endocr Rev 2008;29:677–96.
27. Mankouri J, Tedbury PR, Gretton S, Hughes ME, Griffin SD, Dallas ML, et al. Enhanced hepatitis C virus genome replication and lipid accumulation mediated by inhibition of AMP-activated protein kinase. Proc Natl Acad Sci U S A 2010;107:11549–54.

Published OnlineFirst June 24, 2013; DOI: 10.1158/0008-5472.CAN-13-1429

28. Horman S, Vertommen D, Heath R, Neumann D, Mouton V, Woods A, et al. Insulin antagonizes ischemia-induced Thr172 phosphorylation of AMP-activated protein kinase alpha-subunits in heart via hierarchical phosphorylation of Ser485/491. J Biol Chem 2006;281:5335–40.
29. Hurley RL, Barre LK, Wood SD, Anderson KA, Kemp BE, Means AR, et al. Regulation of AMP-activated protein kinase by multisite phosphorylation in response to agents that elevate cellular cAMP. J Biol Chem 2006;281:36662–72.
30. Djouder N, Tuerk RD, Suter M, Salvioni P, Thali RF, Scholz R, et al. PKA phosphorylates and inactivates AMPKalpha to promote efficient lipolysis. EMBO J 2010;29:469–81.
31. Robey RB, Hay N. Is Akt the "Warburg kinase"?—Akt-energy metabolism interactions and oncogenesis. Semin Cancer Biol 2009;19:25–31.
32. Kim JW, Gao P, Liu YC, Semenza GL, Dang CV. Hypoxia-inducible factor 1 and dysregulated c-Myc cooperatively induce vascular endothelial growth factor and metabolic switches hexokinase 2 and pyruvate dehydrogenase kinase 1. Mol Cell Biol 2007;27:7381–93.
33. Deprez J, Vertommen D, Alessi DR, Hue L, Rider MH. Phosphorylation and activation of heart 6-phosphofructo-2-kinase by protein kinase B and other protein kinases of the insulin signaling cascades. J Biol Chem 1997;272:17269–75.
34. Barthel A, Okino ST, Liao J, Nakatani K, Li J, Whitlock JP Jr, et al. Regulation of GLUT1 gene transcription by the serine/threonine kinase Akt1. J Biol Chem 1999;274:20281–6.
35. Zha X, Wang F, Wang Y, He S, Jing Y, Wu X, et al. Lactate dehydrogenase B is critical for hyperactive mTOR-mediated tumorigenesis. Cancer Res 2011;71:13–8.
36. Semenza GL, Jiang BH, Leung SW, Passantino R, Concordet JP, Maire P, et al. Hypoxia response elements in the aldolase A, enolase 1, and lactate dehydrogenase A gene promoters contain essential binding sites for hypoxia-inducible factor 1. J Biol Chem 1996;271:32529–37.
37. Lunt SY, Vander Heiden MG. Aerobic glycolysis: meeting the metabolic requirements of cell proliferation. Annu Rev Cell Dev Biol 2011;27:441–64.
38. Wang R, Dillon CP, Shi LZ, Milasta S, Carter R, Finkelstein D, et al. The transcription factor Myc controls metabolic reprogramming upon T lymphocyte activation. Immunity 2011;35:871–82.
39. Morani F, Pagano L, Prodam F, Aimaretti G, Isidoro C. Loss of expression of the oncosuppressor PTEN in thyroid incidentalomas associates with GLUT1 plasmamembrane expression. Panminerva Med 2012;54:59–63.
40. Garcia-Cao I, Song MS, Hobbs RM, Laurent G, Giorgi C, de Boer VC, et al. Systemic elevation of PTEN induces a tumor-suppressive metabolic state. Cell 2012;149:49–62.
41. Mihaylova MM, Shaw RJ. The AMPK signalling pathway coordinates cell growth, autophagy and metabolism. Nat Cell Biol 2011;13:1016–23.
42. Hardie DG, Ross FA, Hawley SA. AMPK: a nutrient and energy sensor that maintains energy homeostasis. Nat Rev Mol Cell Biol 2012;13:251–62.
43. Ning J, Xi G, Clemmons DR. Suppression of AMPK activation via S485 phosphorylation by IGF-I during hyperglycemia is mediated by AKT activation in vascular smooth muscle cells. Endocrinology 2011;152:3143–54.
44. Dagon Y, Hur E, Zheng B, Wellenstein K, Cantley LC, Kahn BB. p70S6 kinase phosphorylates AMPK on serine 491 to mediate leptin's effect on food intake. Cell Metab 2012;16:104–12.
45. Faubert B, Boily G, Izreig S, Griss T, Samborska B, Dong Z, et al. AMPK is a negative regulator of the Warburg effect and suppresses tumor growth *in vivo*. Cell Metab 2013;17:113–24.
46. Alaynick WA, Kondo RP, Xie W, He W, Dufour CR, Downes M, et al. ERRgamma directs and maintains the transition to oxidative metabolism in the postnatal heart. Cell Metab 2007;6:13–24.
47. Scarpulla RC. Metabolic control of mitochondrial biogenesis through the PGC-1 family regulatory network. Biochim Biophys Acta 2011;1813:1269–78.
48. Eichner LJ, Perry MC, Dufour CR, Bertos N, Park M, St-Pierre J, et al. miR-378(*) mediates metabolic shift in breast cancer cells via the PGC-1beta/ERRgamma transcriptional pathway. Cell Metab 2010;12:352–61.
49. Hobert JA, Mester JL, Moline J, Eng C. Elevated plasma succinate in PTEN, SDHB, and SDHD mutation-positive individuals. Genet Med 2012;14:616–9.
50. Mutter GL, Lin MC, Fitzgerald JT, Kum JB, Baak JP, Lees JA, et al. Altered PTEN expression as a diagnostic marker for the earliest endometrial precancers. J Natl Cancer Inst 2000;92:924–30.
51. Hong Y, Downey T, Eu KW, Koh PK, Cheah PY. A 'metastasis-prone' signature for early-stage mismatch-repair proficient sporadic colorectal cancer patients and its implications for possible therapeutics. Clin Exp Metastasis 2010;27:83–90.
52. Cai Z, Zhao JS, Li JJ, Peng DN, Wang XY, Chen TL, et al. A combined proteomics and metabolomics profiling of gastric cardia cancer reveals characteristic dysregulations in glucose metabolism. Mol Cell Proteomics 2010;9:2617–28.